ELSEVIER

Journal of Alloys and Compounds 224 (1995) 253–261

Journal of ALLOYS AND COMPOUNDS

Magnetic structures of RNi_2Ge_2 (R = Dy, Ho and Er) and $YbNi_2Si_2$

G. André [a], P. Bonville [b], F. Bourée [a], A. Bombik [c], M. Kolenda [d], A. Oleś [c], A. Pacyna [e], W. Sikora [c], A. Szytula [d,*]

[a] *Laboratoire Léon Brillouin (CEA-CNRS), CEN-Saclay, 91191 Gif-Sur-Yvette, France*

[b] *Direction des Sciences de la Matière, DPhG/SPSRM, Centre d'Etudes Nucléaires de Saclay, 91191 Gif-Sur-Yvette, France*

[c] *Department of Physics and Nuclear Techniques, Academy of Mining and Metallurgy, Reymonta 19, 30-059 Kraków, Poland*

[d] *Institute of Physics, Jagellonian University, Reymonta 4, 30-059 Kraków, Poland*

[e] *Institute of Nuclear Physics, Radzikowskiego 152, 31-342 Kraków, Poland*

Received 3 November 1994; in final form 22 December 1994

Abstract

Results of X-ray, neutron diffraction, Mössbauer effect and magnetometric measurements for RNi_2Ge_2 (R = Dy, Ho and Er) and $YbNi_2Si_2$ compounds are presented. All compounds crystallize in the tetragonal $ThCr_2Si_2$ ($CeAl_2Ga_2$)-type crystal structure and are antiferromagnets with the Néel temperature of 7.5 K for R = Dy, 4.8 K for R = Ho and 3.65 K for R = Er and 2.3 K for $YbNi_2Si_2$. Below T_N a sinemodulated structure with $k = (0, 0, k_z)$ is observed for RNi_2Ge_2 compounds (R = Dy and Er) and with $k = (k_x, k_y, k_z)$ for $HoNi_2Ge_2$. The $YbNi_2Si_2$ has a helicoidal ordering confirmed by the Mössbauer effect data. The Ni atom is non-magnetic and rare earth moments form an angle ϕ with the c-axis which changes from 20° for R = Dy to 90° for $YbNi_2Si_2$. The obtained data are analyzed in terms of the RKKY theory and crystal electric field.

Keywords: Magnetic structures; RKKY theory; Crystal electric field; Rare earths

1. Introduction

Ternary rare earth RT_2X_2 compounds (R = rare earth; T = 3d, 4d or 5d transition metal; X = Si, Ge) were shown to exhibit very exciting physical properties [1]. These intermetallics order magnetically usually at low temperatures and present different types of magnetic structures [1].

The RNi_2X_2 compounds crystallize in the tetragonal $ThCr_2Si_2$ type of structure (see Fig. 1) with the space group $I4/mmm$ [2,3]. Magnetic susceptibility and neutron diffraction data indicate a magnetic ordering at low temperatures [3–11]. The RNi_2Si_2 compounds (R = Pr, Nd, Ho, Er and Tm) have a complex incommensurate antiferromagnetic structure. For $TbNi_2Si_2$ a phase transition between a modulated phase and a simple antiferromagnetic structure, stable at low temperatures, is observed [10]. For $NdNi_2Ge_2$ a modulated antiferromagnetic structure with $k = (0, 0, 0.805)$ below $T_N = 20$ K was found [7]. In the case of $TbNi_2Ge_2$ two transition temperatures are observed: 17 K and 10.25 K [11]. For

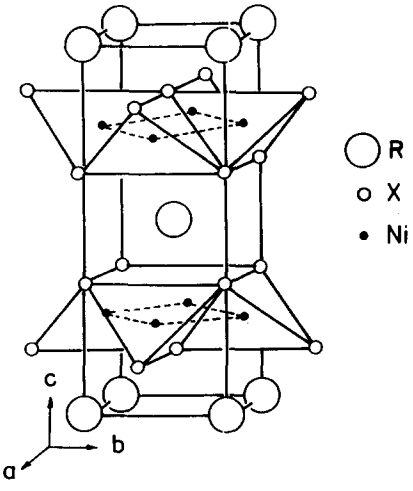

Fig. 1. The crystal structure of RNi_2X_2 compounds.

$HoNi_2Ge_2$ the incommensurate magnetic structure with the propagation vector $k = (0, 0, 0.76)$ is observed below 6 K [6]. A similar type of magnetic ordering was found in $TmNi_2Ge_2$ [8].

We report the results of magnetic susceptibility and neutron diffraction studies on polycrystalline samples

* Corresponding author.

SSDI 0925-8388(95)01545-0

of RNi_2Ge_2 (R = Dy, Ho and Er) and $YbNi_2Si_2$. For $YbNi_2Si_2$, additionally, the Mössbauer effect was studied.

2. Experimental

The polycrystalline materials were prepared by arc melting in an argon atmosphere of stoichiometric amounts of constituent high purity elements (Dy, Ho, Er and Yb-3N, Ni-3N, Si, Ge-4N). The samples were homogenized and annealed for 100 h at 800 °C. The preparation of the $YbNi_2Si_2$ sample is described in [12].

The samples were analyzed by X-ray diffraction using a DRON-3 diffractometer (CuKα). The determined lattice parameters at room temperature (see Table 1) agree with those published earlier [2,3]. The magnetic measurements were carried out using an RH Cahn balance in the temperature range from 2–300 K.

Neutron diffraction data were obtained by means of the powder diffractometer G4.1 installed at the Orphée reactor (Laboratoire Léon Brillouin, Saclay) with an incident neutron wavelength of 2.426 Å, between 2° and 90° in 2θ in the temperature range 1.36–15 K. Neutron scattering lengths were taken from Delapalme [13] and the R^{3+} formfactors were taken from Freeman and Desclaux [14].

The Mössbauer spectra on ^{170}Yb in $YbNi_2Si_2$ were recorded using a linear velocity Doppler drive supporting a neutron activated Tm^*Be_{12} γ-ray source whose linewidth vs. a reference $YbAl_3$ absorber was 2.7 mm s^{-1} (for ^{170}Yb: 1 mm s^{-1} = 68 MHz).

3. Results

3.1. Crystal structure

The neutron diffraction patterns in paramagnetic states (see Figs. 2–5) indicated that all samples exhibit the tetragonal $ThCr_2Si_2$-type crystal structure which belongs to the space group *I4/mmm*. The nuclear intensities were calculated using the following atomic positions:

R in 2(a): 0, 0, 0

Ni in 4(d): 0, 1/2, 1/4; 1/2, 0, 1/4

Ge, Si in 4(e): 0, 0, z; 0, 0, $\bar{z}$,

plus the body centring translation.

The germanium and silicon z positions were refined by the Rietveld profile procedure [15]. The determined values of z parameters are listed in Table 1.

3.2. Magnetic data

The temperature dependence of the magnetic susceptibility of $DyNi_2Ge_2$, $HoNi_2Ge_2$ and $ErNi_2Ge_2$ exhibits maxima at 7.5 K, 4.8 K and 3.65 K respectively (see Fig. 6) which is characteristic of a transition to an antiferromagnetic state. For $YbNi_2Si_2$ no anomaly is observed up to 2 K. Above T_N the magnetic susceptibility is described by the relation $\chi = \chi_0 + C/T - \theta$.

For $YbNi_2Si_2$ the reciprocal magnetic susceptibility obeys the Curie–Weiss law only above 100 K. A deviation from linearity below 100 K is due to crystal-field effects. The plot of χ^{-1} vs. T in the temperature interval 100–300 K given the value of effective magnetic moment (4.59 μ_B) near to the free Yb^{3-} ion value (4.54 μ_B) and paramagnetic Curie temperature $\theta_p = -43$ K. This value is quite large compared to the magnetic ordering temperature thereby indicating the existence of the Kondo effect above 100 K. In the temperature interval 5–40 K the value of θ_p is about −5 K which means that the Kondo effect appears below 40 K.

The values of χ_0, the paramagnetic Curie temperature θ_p and the effective magnetic moments μ_{eff} are given in Table 1.

Table 1
Crystal structure and magnetic data for RNi_2Ge_2 (R = Dy, Ho and Er) and $YbNi_2Si_2$ compounds

Compound	$DyNi_2Ge_2$	$HoNi_2Ge_2$	$ErNi_2Ge_2$	$YbNi_2Si_2$
a (Å)	4.039(2)	4.0290(7)	4.0188(8)	3.9132(5)
c (Å)	9.803(6)	9.7800(27)	9.7688(25)	9.5180(5)
a/c	0.412	0.412	0.411	0.411
V (Å^3)	159.89(26)	158.76(10)	157.77(11)	145.75(4)
z	0.372(10)	0.377(1)	0.376(1)	0.375(1)
T_N (K), M [a], N [b]	7.5, 8.5	4.8, 4.1	3.65, 3.1	2.1 [c], 2.3
θ_p (K)	−3.1	1.0	1.4	−43.0
μ_{eff} (μ_B), exp, theor	10.78, 10.65	10.27, 10.61	9.49, 9.72	4.59, 4.54
$\chi_0 \times 10^6$ (cm^3 g^{-1})	3.22	1.77	7.17	6.0
$\mu_n(\mu_B)$, exp, theor	7.8(1), 10	9.96(5), 10	8.30(5), 9	1.8, 4
ϕ (°) [d]	20	42	64	90

[a] M, the value determined from the magnetic data.

[b] N, the value determined from teh neutron diffraction data.

[c] From the Mössbauer effect data [12].

[d] ϕ, angle between direction of the magnetic moment and c-axis.

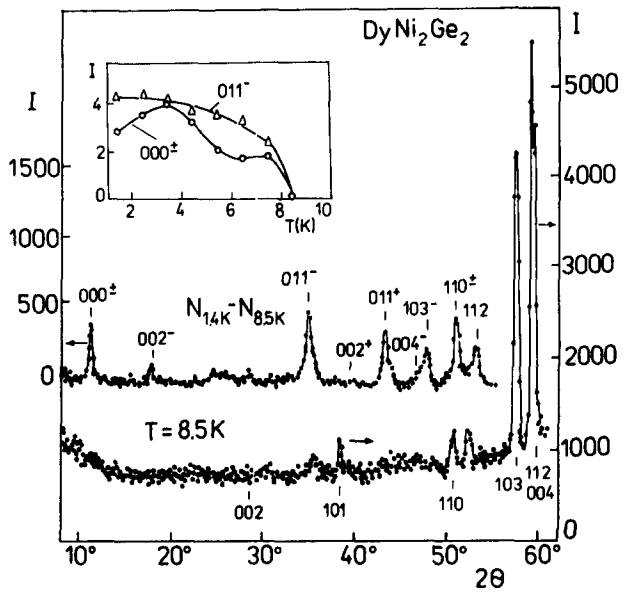

Fig. 2. Neutron diffraction pattern of $DyNi_2Ge_2$ at 8.5 K and magnetic diffraction pattern as a difference between the patterns at 1.4 and 8.5 K. The temperature dependence of the magnetic intensities of $000^{\pm}$ and 011^{-} reflections are shown in the inset.

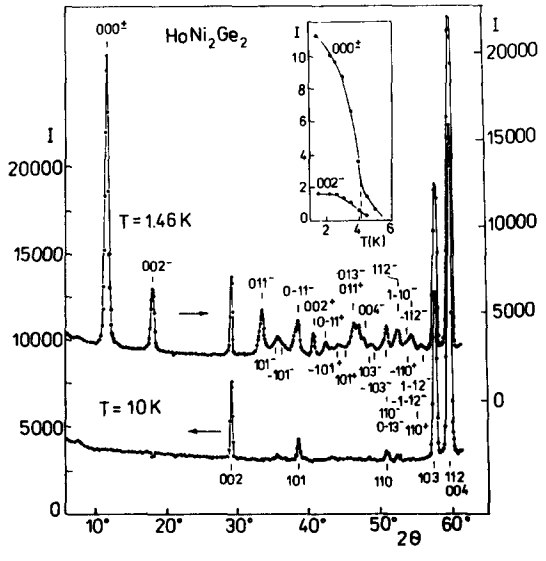

Fig. 3. Neutron diffraction patterns of $HoNi_2Ge_2$ at 1.46 and 10 K. Inset shows the temperature dependence of $000^{\pm}$ and 002^{-} magnetic peaks.

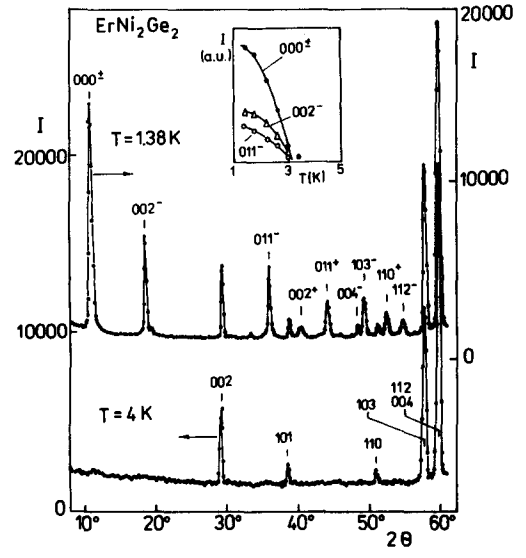

Fig. 4. Neutron diffraction patterns of $ErNi_2Ge_2$ at 1.38 and 4 K. Inset shows the temperature dependence of $000^{\pm}$, 002^{-} and 011^{-} magnetic peaks.

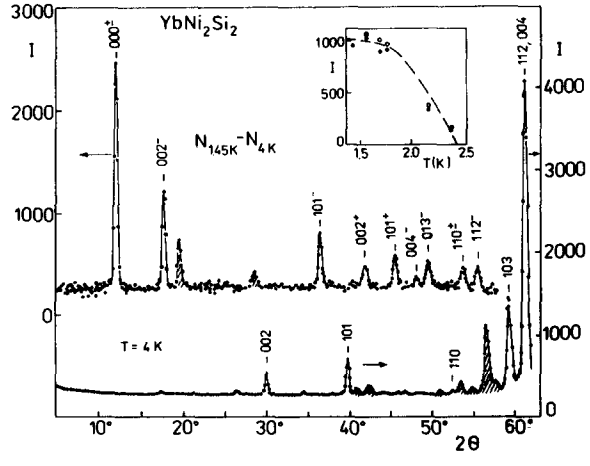

Fig. 5. Neutron diffraction patterns of $YbNi_2Si_2$ at 4 K and magnetic diffraction pattern as a difference between the patterns taken at 1.45 and 4 K. The shaded peaks correspond to a impurities. The inset shows the temperature dependence of $000^{\pm}$ magnetic peak.

3.3. Magnetic structure

3.3.1. $DyNi_2Ge_2$

The low temperature neutron diffractogram (at $T=1.4$ K) of the $DyNi_2Ge_2$ compound contains several additional reflections (see Fig. 2). Their positions are incommensurate with regard to the nuclear lines and they can be indexed considering the propagation vector $k=(0, 0, k_z)$ with $k_z=0.788$. The absence of high order nk_z satellites and the lack of a ferromagnetic contribution to the nuclear peaks, a square modulated or a conical magnetic structure is excluded but a spiral or a sine modulated structure may be considered. The existence of the magnetic peak $(002)^{-}$ indicates that the magnetic moment forms an angle ϕ with the c-axis. The intensities of the magnetic peaks are calculated using the method reported in [16]. The best fit was obtained for the model of a modulated structure (see Fig. 7(a)). The magnetic moment equals 7.8(1) μ_B at $T=1.4$ K and forms an angle $\phi=20°$ with the c-axis. The observed and calculated magnetic intensities are compared in Table 2.

The temperature dependence of the $000^{\pm}$ and 011^{-} magnetic reflections gives the Néel temperature to be 8.5 K (see Fig. 2).

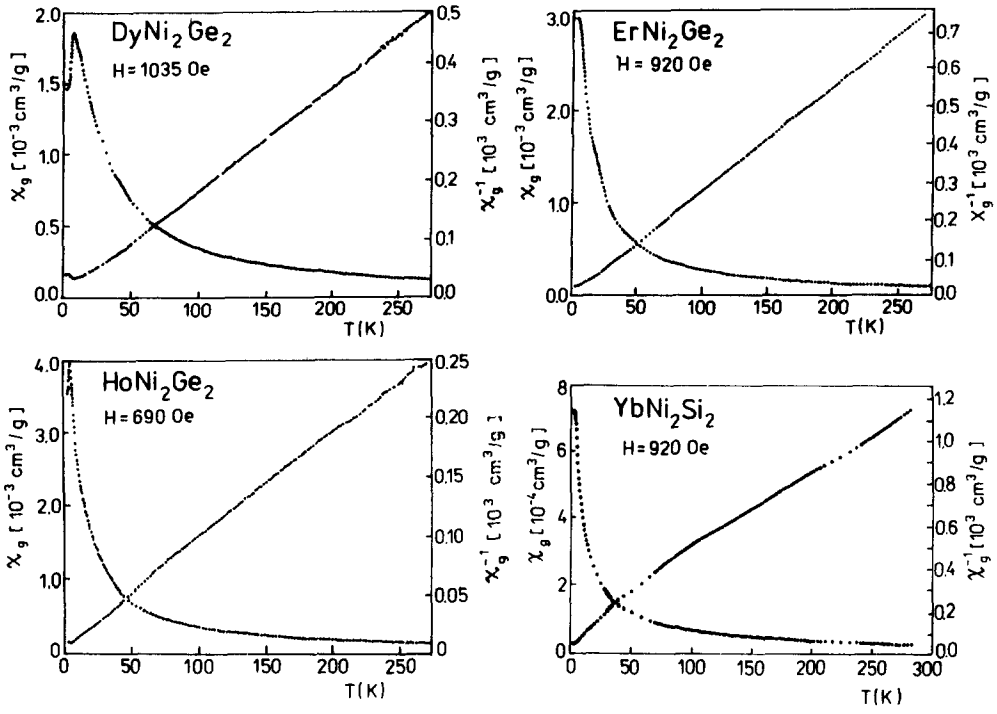

Fig. 6. Temperature dependence of the magnetic susceptibility and the reciprocal susceptibility of $DyNi_2Ge_2$, $HoNi_2Ge_2$, $ErNi_2Ge_2$ and $YbNi_2Si_2$.

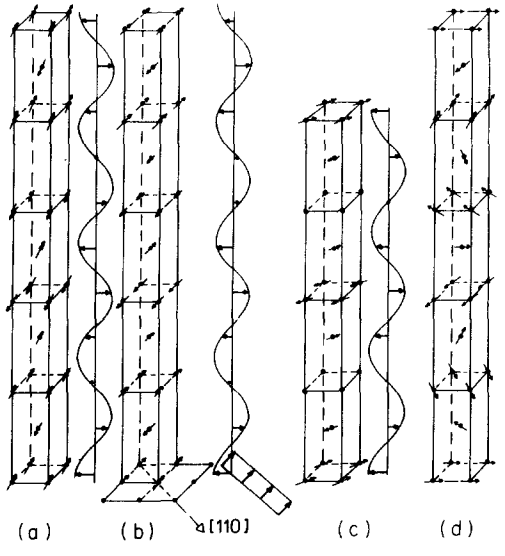

Fig. 7. Modulated magnetic structures of (a) $DyNi_2Ge_2$, (b) $HoNi_2Ge_2$, (c) $ErNi_2Ge_2$ and (d) $YbNi_2Si_2$.

Table 2
Bragg angles and integrated magnetic intensities for $DyNi_2Ge_2$

$h\ k\ l$	$2\theta_{calc}$	$2\theta_{obs}$	I_{calc} (H)	I_{calc} (MS)	I_{obs}
0 0 $0^{\pm}$	11.3	11.3	121.0	55.0	59.4
0 0 2^{-}	17.4	17.4	50.5	23.0	9.1
1 0 1^{-}	35.2	35.3	43.2	73.5	144.1
0 1 1^{-}			25.1	83.0	
0 0 2^{+}	40.8	–	8.3	3.8	–
1 0 1^{+}	44.0	44.1	22.1	31.4	75.5
0 1 1^{+}			14.9	35.2	
0 0 4^{-}	47.3	–	5.9	2.7	–
1 0 3^{-}	48.2	48.2	16.9	22.3	51.3
0 1 3^{-}			12.0	21.9	
1 1 $0^{\pm}$	51.8	51.9	28.5	63.7	64.0
1 1 2^{-}	53.8	53.9	35.5	55.1	55.6
R (%)			68.3	11.2	

3.3.2. $HoNi_2Ge_2$

Additional reflections in the neutron diffraction pattern at $T=1.46$ K could be successfully interpreted as satellite pairs associated with reciprocal lattice points (Fig. 3). These reflections were indexed using a computer program [16]. A modulated magnetic structure with a propagation vector $k=(0.014, 0.073, 0.784)$ was derived.

The best fit to the experimental data was obtained for the model of a modulated magnetic structure. The magnetic moment equal to 9.96(5) μ_B forms an angle 42° with the c-axis (see Fig. 7(b)). A comparison of the calculated and observed intensities are given in Table 3.

The temperature dependence of the $000^{\pm}$ and 002^{-} reflections gives the Néel temperature $T_N=4.1$ K (Fig. 3).

3.3.3. $ErNi_2Ge_2$

The neutron diffraction diagram of $ErNi_2Ge_2$ taken at 1.38 K compared to that at $T=4$ K shows additional peaks (Fig. 4). These peaks have been indexed with a propagation vector $k=(0, 0, 0.757)$. The best fit to the experimental data was obtained for the model of

Table 3
Bragg angles and integrated magnetic intensities for $HoNi_2Ge_2$

h k l	$2\theta_{calc}$	$2\theta_{obs}$	I_{calc} (H)	I_{calc} (MS)	I_{obs}
0 0 0±	11.5	11.7	528.0	531.2	538.9
0 0 2⁻	17.8	18.1	172.9	138.2	114.6
0 1 1⁻	32.8	33.3	85.3	92.8	105.9
1 0 1⁻	35.1	35.6	40.7	62.2	83.3
−1 0 1⁻	36.1		39.2	41.6	
0 −1 1⁻	38.2	38.6	61.5	64.5	60.0
0 0 2⁺	40.6	40.6	33.0	30.4	28.8
0 −1 1⁺	42.0	42.3	35.1	33.0	28.0
−1 0 1⁺	43.8	44.1	24.4	7.8	47.3
1 0 1⁺	44.7		26.6	50.2	
0 1 1⁺	46.4	46.2	41.2	45.1	140.8
0 1 3⁻	46.6	46.9	37.0	39.9	
0 0 4⁻	47.2	47.5	21.7	18.5	
1 0 3⁻	48.1	48.7	21.5	42.5	
−1 0 3⁻	48.9		19.2	2.8	
1 1 0⁻	50.0	50.8	27.0	27.2	70.0
0 −1 3⁻	50.5		22.4	20.1	
−1 1 0⁻	50.7		22.1	22.0	
1 1 2⁻	51.9	52.3	27.7	31.4	70.4
−1 1 2⁻	52.7		21.3	25.4	
−1 1 0⁺	53.9	54.3	21.2	28.4	72.0
1 1 0⁺	54.6		25.9	26.1	
1 −1 2⁻	55.7	55.7	19.8	9.6	3.9
−1 −1 2⁻	56.4		16.7	30.3	
R (%)			13.1	11.3	

Table 4
Bragg angles and integrated magnetic intensities for $ErNi_2Ge_2$

h k l	$2\theta_{calc}$	$2\theta_{obs}$	I_{calc} (H)	I_{calc} (MS)	I_{obs}
0 0 0±	10.8	10.84	448.93	449.16	455.57
0 0 2⁻	17.9	18.4	159.30	159.38	139.67
0 0 2⁺	40.1	40.2	29.38	29.39	30.57
1 0 1⁻	35.7	35.8	64.53	75.96	112.07
0 1 1⁻	35.7		47.06	37.21	
1 0 1⁺	44.0	44.0	42.60	47.28	79.45
1 0 0⁺	44.0		34.26	30.28	
0 0 4⁻	47.8	48.2	20.06	20.07	24.69
1 0 3⁻	49.0	49.1	35.08	38.24	71.0
0 1 3⁻	49.0		41.42	32.75	
1 1 0±	52.3	52.3	49.16	49.81	52.57
1 1 2⁻	54.6	54.6	45.91	46.48	42.32
1 1 2⁺	66.8	66.5	31.88	32.13	35.27
1 0 3⁺	67.8	67.6	17.60	18.45	36.00
0 1 3⁺	67.8		16.32	15.61	
R_M (%)			4.92	4.34	

Table 5
Bragg angles and integrated magnetic intensities for $YbNi_2Si_2$

h k l	$2\theta_{calc}$	$2\theta_{obs}$	I_{calc} (MS)	I_{calc} (H)	I_{obs}
0 0 0	11.7	11.7	1032	1036	1086
0 0 2⁻	17.5	17.6	447	448	488
0 1 1⁻	36.3	36.2	166	330	312
1 0 1⁻	36.3		166	2	
0 1 1⁺	45.4	45.4	104	160	208
1 0 1⁺	45.4		104	56	
0 0 4⁻	48.0	48.0	60	60	99
0 1 3⁻	49.4	49.4	94	130	236
1 0 3⁻	49.4		94	58	
1 1 0±	53.6	53.6	144	144	128
1 1 2⁻	55.4	55.4	120	120	136
R (%)			9.0	9.1	

a modulated structure. The magnetic moment of erbium atoms equal to 8.3(3) μ_B forms an angle 64° with the c-axis. In this case the disagreement is $R=4.3$. A similar value of the R factor is $R=4.9$ which is obtained for the model of a helicoidal structure. A comparison of magnetic intensities observed and calculated for both models is presented in Table 4. The temperature dependence of the 000±, 002⁻ and 011⁻ reflections gives the Néel temperature 3.1 K (see Fig. 4).

3.3.4. $YbNi_2Si_2$

In the neutron diffraction pattern at 1.43 K the additional peaks of the magnetic origin are observed. These peaks were indexed with the wavevector $k=(0, 0, 0.8025)$. A comparison of the experimental and calculated data gives similar values of the disagreement factor for a helicoidal and a sinemodulated structures. In both cases the magnetic moment is perpendicular to the c-axis. A comparison of both calculated models with the observed magnetic intensities is given in Table 5. It is not possible to get an univocal model of the magnetic structure of $YbNi_2Si_2$ basing only on the neutron diffraction data.

The ^{170}Yb Mössbauer absorption spectra [12] give more information about the magnetic structure of the magnetically ordered phase of $YbNi_2Si_2$. The hyperfine field, proportional to the magnetic moment, is found to be perpendicular to the main axis of the electric field gradient tensor at the Yb site, i.e. the crystal c-axis. As it was mentioned above in both magnetic structure models derived from the neutron diffraction analysis the magnetic moments of Yb ions are also perpendicular to the c-axis. The Mössbauer spectral shape can further help choosing between the two models: at $T=1.43$ K, model 1 implies that all the Yb moments are equal (≈ 1.3 μ_B) and form helicoidal magnetic structures, whereas model 2 presents the sinemodulated magnetic structure with $m_0 \approx 1.8$ μ_B. Simulated Mössbauer absorption spectra according to both models at $T=1.43$ K are represented in Fig. 8. The experimental absorption spectrum at $T=1.35$ K is shown in Fig. 9. Although the line broadenings of the experimental spectrum are inhomogeneous, due to a small distribution

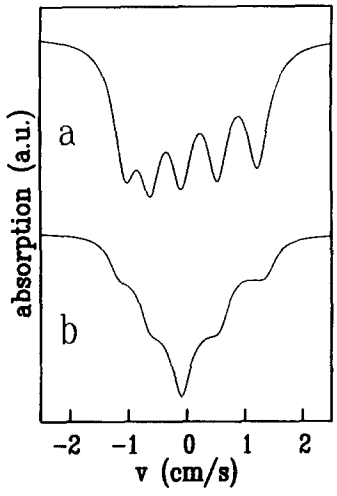

Fig. 8. Simulations of the ^{170}Yb Mössbauer absorption spectrum according to: (a) the helicoidal magnetic structure (model 1) and (b) the sinemodulated magnetic structure (model 2) of $YbNi_2Si_2$ at $T=1.45$ K.

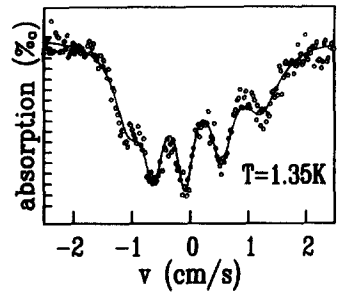

Fig. 9. ^{170}Yb Mössbauer absorption spectrum in $YbNi_2Si_2$ at $T=1.35$ K.

of hyperfine parameters, it is clear that experiment favours model 1, i.e. the helicoidal magnetic structure. It can be noticed that the magnitude of the Yb magnetic moment, derived from the hyperfine field value at 1.35 K, is: $m=1.47(3)$ μ_B, and it is 10% higher than the moment derived from the neutron pattern taken at 1.45 K.

4. Symmetry analysis

The magnetic representation d_M for the *I4/mmm* (D^{17}_{2h}) symmetry group and 2(a) positions of magnetic atoms and $k=(0, 0, k_z)$ can be presented as a direct sum of two irreducible representations: one dimensional τ_2 and two dimensional τ_5.

The calculated [17] magnetic modes are presented in Table 6.The possible magnetic structures are:for representation τ_2 and mixing coefficients giving the order parameter $p=(c,-c)$,

$$S_{1+t}=2ce_z\cos(\bar{k}\cdot\bar{t})$$
$$S_{2+t}=2ce_z\cos(\pi k_z+\bar{k}\cdot\bar{t}) \quad (1)$$

Table 6
Modes belonging to the τ_2 and τ_5 representations of the I4/mmm (D^{17}_{2h}) group and $k=(0,0,k_z)$, $k_z=\mu$ and 2(a) positions

			1:(0, 0, 0)	2:(0.5, 0.5, 0.5)
k_1	τ_2	Ψ_1	(0, 0, 1)	(0, 0, $\exp(i\pi\mu)$)
	τ_5	Ψ_1	(1, $-i$, 0)	($\exp(i\pi\mu)$, $-i\exp(i\pi\mu)$, 0)
		Ψ_2	(1, i, 0)	($\exp(i\pi\mu)$, $i\exp(i\pi\mu)$, 0)
k_2	τ_2	Ψ_1	(0, 0, -1)	(0, 0, $-\exp(-i\pi\mu)$)
	τ_5	Ψ_1	(1, i, 0)	($\exp(-i\pi\mu)$, $i\exp(-i\pi\mu)$, 0)
		Ψ_2	(1, $-i$, 0)	($\exp(-i\pi\mu)$, $-i\exp(-i\pi\mu)$, 0)

for representation τ_5 and mixing coefficients giving the order parameter $p=(c, 0; c, 0)$,

$$S_{1+t}=2c[e_x\cos(\bar{k}\cdot\bar{t})+e_y\sin(\bar{k}\cdot\bar{t})]$$
$$S_{2+t}=2c[e_x\cos(\pi k_2+\bar{k}\cdot\bar{t})+e_y\sin(\pi k_2+\bar{k}\cdot\bar{t})] \quad (2)$$

$$p=(c, c; c, c),$$
$$S_{1+t}=2ce_x\cos(\bar{k}\cdot\bar{t})$$
$$S_{2+t}=2ce_x\cos(\pi k_2+\bar{k}\cdot\bar{t}) \quad (3)$$

$$p=(ic, -ic; -ic, ic),$$
$$S_{1+t}=2ce_y\cos(\bar{k}\cdot\bar{t})$$
$$S_{2+t}=2ce_y\cos(\pi k_2+\bar{k}\cdot\bar{t}) \quad (4)$$

As can be seen from the equations that along the z-axis only a modulated structure is possible while in the xy-plane a spiral structure or a modulated structure are possible but the latter should be directed along the one of coordinate axes.

The best agreement between calculated and measured diffraction patterns takes place for magnetic structure described using Eqs. (1), (3) or (4) for $DyNi_2Ge_2$ and $ErNi_2Ge_2$ and Eq. (2) for $YbNi_2Si_2$. The magnetic structures of $HoNi_2Ge_2$ are described by the wave vector $\bar{k}=(k_x, k_y, k_z)$. In this case the symmetry analysis gives only modulated structures:

$$S_{1+t}=2c(e_x\pm e_y)\cos(\bar{k}\cdot\bar{t})$$
$$S_{2+t}=2c(e_x\pm e_y)\cos(\bar{k}\cdot\bar{t}+\pi k_z) \quad (5)$$

or

$$S_{1+t}=2ce_z\cos(\bar{k}\cdot\bar{t})$$
$$S_{2+t}=2ce_z\cos(\bar{k}\cdot\bar{t}+\pi k_z) \quad (6)$$

5. Discussion

All compounds investigated in this work crystallize into the body-centered tetragonal $ThCr_2Si_2$-type structure. The atomic framework of the $ThCr_2Si_2$-type structure (see Fig. 1) can be displayed as a sequence of planes of the same atoms R–X–T–X–R–X–T–X–R per-

pendicular to the c-axis. Interatomic distances between rare earth atoms in the planes are about 4 Å whereas between planes the distance is near 5.65 Å.

The magnetic moments in the compounds discussed in this work are almost exclusively due to localized 4f electrons. The values of effective moments deduced from the temperature dependence of the magnetic susceptibility are close to the theoretical values for free R^{3+} ions (see Table 1).

In an ordered state the magnetic moments of holmium and erbium atoms are near to the free R^{3+} ion value gJ, whereas those of dysprosium and ytterbium are considerably smaller.

The particular location of the rare earth atoms in the crystal structure of $ThCr_2Si_2$-type is responsible for the anisotropic character of the magnetic interaction between the magnetic moments of the rare earth atoms. RNi_2Ge_2 compounds have a sine modulated structure and $YbNi_2Si_2$ has a helicoidal order. The determined magnetic structures indicate that exchange interactions J_0 within the (00l) plane are strongly ferromagnetic, whereas the couplings J_1 and J_2, between planes are weaker and can be antiferromagnetic.

All determined magnetic structures are described by the wavevector $\bar{k}=(0, 0, k_z)$ with k_z being between 0.5 and 1.0. This type of magnetic structure being a cosinusoidally modulated longitudinal spin wave LSWI [1]. The magnetic phase diagram is shown in Fig. 10 [1,18,19]. The proposed model [18] indicates that:

- for positive or negative values of J_2 exchange integral and $J_2<J_1/4$ a simple ferro- or antiferro AF I magnetic structure is stable;
- for $J_1/4<J_2<J_1/2$ the modulated magnetic ordering with a wavevector $\bar{k}=(0, 0, k_z)$ is stable. The values of the k_z component are given by the relation $\cos \pi k_z = -J_1/4J_2$. The relation is fulfilled in two regions (see Fig. 10) with the different values of k_z component. For the compounds measured $0.5<k_z<1.0$ which indicates that both J_1 and J_2 integrals are negative;
- for $J_2>J_1/4$ the antiferromagnetic AF II structure is stable.

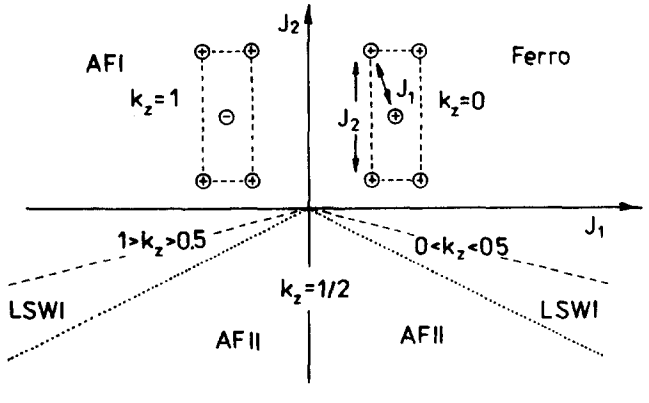

Fig. 10. Stability conditions of the RT_2X_2 ternary compounds for the exchange integrals J_1 and J_2 (Ising model) [18,19].

The observed modulated character of magnetic orderings indicates that they are stabilized by long range interactions, probably of the RKKY-type. In the RKKY model of isostructural series of compounds, the paramagnetic Curie temperature θ_p or the magnetic ordering temperatures T_N or T_C should be proportional to the de Gennes function $G=(g-1)^2J(J+1)$ [20]. The results for RNi_2Si_2 and RNi_2Ge_2 compounds presented in Fig. 11 indicate that the de Gennes scaling is obeyed except for the Tb-compounds. It means that the RKKY interactions are very probable and that the crystal electric field plays an important role in these interactions.

The stability of the magnetic scheme was discussed first in terms of an isotropic RKKY mechanism along, and then together with the crystal field effects.

In an isotropic RKKY model the Fermi vector is given by the formula $k_F=6Za/\pi c$ where Z is the number of free electrons per magnetic ion and c/a is the ratio of lattice parameters. The analysis of a/c ratios for a number of RT_2X_2 compounds indicates that for $a/c>0.408$ an oscillatory magnetic ordering scheme appears in the crystal [1]. For all investigated compounds the condition $a/c>0.408$ is fulfilled (see Table 1).

In the RKKY theory the paramagnetic Curie temperature θ_p is given by the following formula:

$$\theta_p = \frac{-3\pi z^2}{k_B E_F} \Omega^{-2} J_{sf}^2 (g_J-1)^2 J(J+1) \Sigma F(2k_F R_{ij}) \qquad (7)$$

where Ω is the atomic volume, Z is the number of conduction electrons per rare earth atom, E_F is the Fermi energy, J_{sf} is the RKKY exchange integral and $F(x)=(x\cos x-\sin x)/x^4$. The stable modulated magnetic structure described by a wave vector $k=(0, 0, k_z)$ is

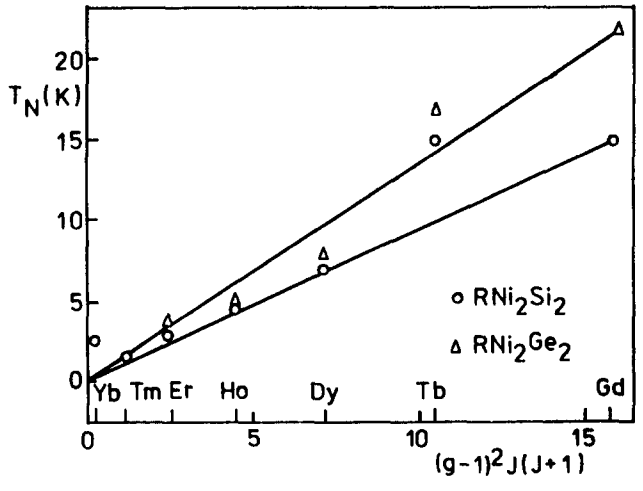

Fig. 11. The Néel temperatures of RNi_2Si_2 and RNi_2Ge_2 compounds as a function of the rare earth atoms. The solid line represents the de Gennes scaling.

the one for which the energy of the system is minimal. The formula for the Néel temperature is

$$T_N = -\frac{3\pi z^2}{k_B E_F}\Omega^{-2} J_{sf}^2 (g_J-1)^2 J(J+1) \times \Sigma F(2k_F R_{ij})\cos(kR_{ij}) \quad (8)$$

The RKKY sums, $\Sigma F(2k_F R_{ij})$ and $\Sigma F(2kFR_{ij})\cos(kR_{ij})$ for $ErNi_2Ge_2$, taken over all Er sites inside the sphere of the radius 100 Å, are shown in Fig. 12. Since the paramagnetic Curie temperature is positive, the sums in Eqs. (7) and (8) satisfy the relation $\theta_p > 0$ and $T_N > 0$ and lead to the following values of k_F vector: 0.6 $Å^{-1} > k_F > 0.85$ $Å^{-1}$ and 1.45 $Å^{-1} > k_F > 1.75$ $Å^{-1}$ which correspond to Z equal $0.278 < Z < 0.78$ and $3.8 < Z < 6.8$. The first region does not make physical sense. The second shows that the $5d4s^2$ electrons of rare earth atoms and also partially $4s^2$ electrons of Ni atoms together $4s^24p^2$ electrons of Ge atoms contribute to the conduction electron bands.

The interaction of crystalline electric fields (CEF) with the multiple moments of R atom electrons at a site of a crystal lattice of 4/*mmm* point symmetry is given by the hamiltonian

$$H_{CF} = B_2^0 O_2^0 + B_4^0 O_4^0 + B_4^4 O_4^4 + B_6^0 O_6^0 - B_0^4 O_6^4 \quad (9)$$

where O_m^n is the Stevens operator, B_n^m is a CEF parameter defined by Hutchings [21]. The determined values of B_n^m parameters described in the work [22] indicate that the B_2^0 parameter is dominant since the others are smaller by an order of magnitude. Łątka [23] and Blanco et al. [24] determined the values of B_2^0 parameters for different RNi_2Si_2 compounds. The results are collected in Table 7.

At a site of the tetragonal point symmetry, the magnetic moment is parallel to the *c*-axis if B_2^0 is negative and it is perpendicular to the *c*-axis if B_2^0 is positive [25], provided the effect of the second-order B_2^0 parameter is dominant. The signs of the B_2^0 coefficients with the orientation of the magnetic moments deduced from the neutron diffraction experiments are collected in Table 7. For RNi_2Si_2 compounds the disagreement is observed only for $HoNi_2Si_2$. In this case, the value of B_2^0 is very small, thus, crystal field terms of higher order can prevail.

For RNi_2Ge_2 germanides the values of the B_2^0 parameters have not been determined. In the RNi_2Ge_2 series a change in the direction of the magnetic moments is observed. For $TbNi_2Ge_2$ the magnetic moment is parallel to the *c*-axis [6,11]. In compounds with the Dy, Ho and Er investigated in this work the magnetic moments form an angle ϕ with the *c*-axis. The value of the angle increases with an increase in the number of f-electrons. For $TmNi_2Ge_2$ [8] the magnetic moment is perpendicular to the *c*-axis.

According to Sanchez et al. [26] the canting angle ϕ is connected with the value of the B_4^0 term. The determined values of all B_n^m parameters for $TbNi_2Si_2$ compound [24] indicate that the B_4^0 is small (5.57×10^{-4} K) and it changes slightly with the change in f-electrons, for example for $PrNi_2Si_2$ it equals 4.6×10^{-3} K [23]. With an increase in the number of f-electrons the values of the B_2^0 parameters decrease. The observed change in the ϕ angle is connected with the change in the two B_2^0 and B_4^0 parameters. A formula for the angle ϕ for compounds with tetragonal symmetry is given in [27].

$$\phi = \frac{1}{J}\sqrt{\frac{3}{7}J(J+1) - \frac{3}{70}\left(\frac{B_2^0}{B_4^0}\right)} \quad (10)$$

Table 7 presents the calculated values of the B_2^0/B_4^0 ratio for germanides. It is seen that for the Tb-, Dy- and Ho-compounds the sign of the B_2^0/B_4^0 ratio is negative, while for the Er-, Tm- and Yb-compounds it is positive. Because the B_4^0 parameter is positive [24] a change in the sign of the B_2^0/B_4^0 ratio depends on the sign of the B_2^0 parameter. The values of the B_2^0/B_4^0 ratio for germanides show the same dependence that the B_2^0 parameter for silicides. With increase in the number of f-electrons the sign of B_2^0 parameter for the compounds containing Ho and Er changes. The

Table 7
Values of the B_2^0 crystal electric field parameters for RNi_2Si_2 and B_2^0/B_4^0 ratio for RNi_2Ge_2 compounds and direction of the magnetic moments of RNi_2X_2 compounds

R	B_2^0 (K) for silicides	B_2^0/B_4^0 for germanides	Moment direction	
			silicides	germanides
Tb	−0.66[20], −0.96[21]	−420.0	∥ c[10]	∥ [11] ϕ (this work)
Dy	−0.39[20]	−521.5	⊥ [10]	⊥ [6], ϕ (this work)
Ho	−0.13[20]	−104.5	⊥ [10]	ϕ (this work)
Er	+0.14[20]	+385.5	⊥ [10]	⊥ [8]
Tm	+0.55[20]	+420.0	⊥ (this work)	
Yb	+1.65[20]	+157.5		

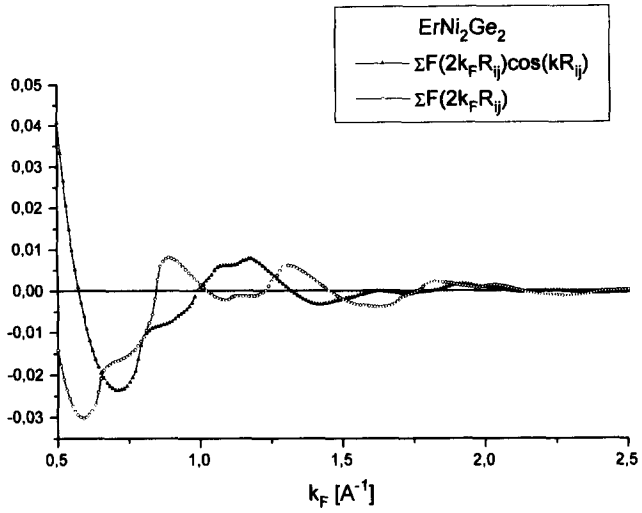

Fig. 12. Dependence of the RKKY sums $\Sigma F(k_F R_{ij})$ and of $\Sigma F(k_F R_{ij}) \cos(kR_{ij})$ as a function of the Fermi vector k_F.

experimental data presented in this work show to what extend the crystal electric field affects the magnetic structure of RT_2X_2 compounds.

Acknowledgements

This work has been partially supported by the State Committee for Scientific Research in Poland from the statutory fund of the Institute of Physics of the Jagellonian University and with Grant 2P302 107 07.

References

[1] A. Szytuła and J. Leciejewicz, in *Handbook on the Physics and Chemistry of Rare Earths*, North Holland, Amsterdam, Vol. 12, 1989, p. 133.

[2] O.I. Bodak, E.I. Gladyschevskii and P.I. Kripyakevich, *Izv. Akad. Nauk. SSSR, ser. Neorgan. Materiały, 2* (1966) 2151.

[3] W. Rieger and E. Parthé, *Monatsh Chem., 100* (1969) 444.

[4] J.K. Yakinthos and P.F. Ikonomou, *Solid State Commun., 34* (1980) 777.

[5] V.N. Nguyen, F. Tcheou, J. Rossat-Mignod and R. Ballestracci, *Solid State Commun., 57* (1986) 941.

[6] H. Pinto, M. Melamud, M. Kuznietz and H. Shaked, *Phys. Rev. B, 31* (1985) 508.

[7] A. Szytuła, A. Oleś, Y.Allain and G. André, *J. Magn. Magn. Mater., 75* (1988) 298.

[8] J.K. Yakinthos, *J. Magn. Magn. Mater., 99* (1991) 123.

[9] J.M. Barandiaran, D. Gignoux, D. Schmitt and J.C. Gomez Sal, *Solid State Commun., 57* (1986) 941.

[10] J.M. Barandiaran, D. Gignoux, D. Schmitt, J.C. Gomez Sal and J. Rodriquez Fernandez, *J. Magn. Magn. Mater., 69* (1987) 61.

[11] F. Bourée-Vigneron, *Phys. Scr., 44* (1991) 27.

[12] P. Bonville, J.A. Hodges, P. Imberto, G. Jéhanno, D. Jaccard and J. Sierro, *J. Magn. Magn. Mater., 97* (1991) 178.

[13] A. Delapalme, *Rap. Interne*, CEA-CNRS/DPh.G.SDN/LLB/85/59.

[14] A.J. Freeman and J.P.Desclaux, *J. Magn. Magn. Mater., 12* (1979) 11.

[15] H.M. Rietveld, *J. Appl. Crystallogr., 2* (1969) 65.

[16] Z. Tomkowicz, *Jagel. Univ. Acta Sci. Lit.* Schedae Physicas, Fasc., 1979, p. 16.

[17] W. Sikora, *Workshop on Magnetic Structures and Phase Transitions, Kraków, August 27–29, 1994*, p. 93.

[18] A. Szytuła, W. Bażela and J. Leciejewicz, *Solid State Commun., 48* (1983) 1053.

[19] R. Welter, *Thesis*, University of Nancy, 1994.

[20] P.G. de Gennes, *J. Phys. Radium, 23* (1962) 510; 630.

[21] M.T. Hutchings, in Seits and D. Turnbull (eds.), *Solid State Physics*, Academic, New York, Vol. 16, 1964, p. 227.

[22] A. Szytuła and J. Leciejewicz, *Handbook Crystal Structures and Magnetic Properties of Rare Earth Intermetallics*, CRC, Boca Raton.

[23] K. Łątka, *Rep. INP*, 1443/PS, Kraków, 1989.

[24] J. Blanco, D. Gignoux, J.C. Gomez-Sal and D. Schmitt, *J. Magn. Magn. Mater., 104–107* (1992) 1273.

[25] J.E. Greedan and V.U.S. Rao, *J. Solid State Chem., 6* (1973) 387; *8* (1973) 386.

[26] J.P. Sanchez, K. Tomala and R. Kmieć, *J Phys., 49* (1988) C8–C435.

[27] Z. Żołnierek and J. Mulak, *J. Magn. Magn. Mater., 140–144* (1995) 1393.